Density functional study of hydrogen adsorption at low temperatures

Chong Gu, Guang-Hua Gao,[a] and Yang-Xin Yu
Department of Chemical Engineering, Tsinghua University, Beijing, 100084, China

(Received 13 January 2003; accepted 8 April 2003)

In substitution of path integral isomorphism of the quantum particle, an effective polymer ring model is proposed in the density functional calculation for hydrogen adsorption in single-walled carbon nanotubes. The excess intrinsic Helmholtz energy for quantum particles includes contributions from hard-sphere repulsion, interatomic bonding and soft attraction. The first two contributions are considered through the method developed by Yu and Wu [J. Chem. Phys. **117**, 2368 (2002)], and the last contribution is obtained from mean field approximation using Weeks–Chandler–Anderson potential. The theoretical predictions are in good agreement with Monte Carlo simulation data for the density distributions of the hydrogen molecule inside the tube. In addition, the proposed model is applied to the calculation of the adsorption isotherms of hydrogen at 100 and 150 K. The present model is simpler than the current existing theories for quantum fluids. © *2003 American Institute of Physics.* [DOI: 10.1063/1.1578614]

I. INTRODUCTION

Hydrogen is a renewable and environmentally friendly energy source and its use in fuel cells for power generation is promising. Storage of hydrogen is a key technique in this application. Carbon nanotubes are now considered as probable hydrogen sorbent. Tremendous efforts have been made over the past ten years to understand the adsorptive ability of carbon nanotubes, including experiments,[1,2] computer simulations,[3–7] and theoretical calculations.[8,9] Darkrim *et al.*[10] reviewed the existing experiments and simulations of hydrogen uptake in carbon nanotubes. Concluded from the data presented in their work, the values of hydrogen adsorption by different authors are relatively scattered. However, so far, few promising results are reported on hydrogen adsorption in carbon nanotubes.

To make a comprehensive understanding of hydrogen storage, adsorption at very low temperature should also be considered. It is evident that, due to the suppressant of the thermal motion of fluid molecules at low temperature, the adsorption can be enhanced. In this situation, the de Broglie wavelength of hydrogen molecule is comparable with its diameter, so hydrogen should be treated quantum mechanically. The standard technique for simulating a quantum fluid at finite temperature is to use the path integral (PI) formalism of Feynman.[11] Feynman established the isomorphism between a quantum particle and a classical ring polymer of P beads, with bounded beads connected by harmonic springs. Computer simulations[3,12] have been carried out to investigate the hydrogen adsorption in single-walled carbon nanotubes (SWNTs) via path integral method.

Other than computer simulation, density functional theory (DFT) is an effective approach to calculate the equilibrium thermophysical properties. While, few work have been done on DFT of quantum fluids. Haymet *et al.*[13–15] have made a series of investigations on quantum DFT of freezing. By choosing a new ideal system, their theory combines density functional techniques with the Feynman path integral formulation of quantum mechanics, which includes correctly the quantum dispersion effects. Their theory applies successfully in the calculation of the phase diagram of helium at low temperatures. In their work, to express the singlet density distribution explicitly, a parabolic form approximation has to be made to represent the relation between the lattice point and the effective potential. However, this relation becomes invalid in an inhomogeneous quantum fluid system as studied in this work. Therefore, it is impossible to apply their work directly in our investigation.

As for a quantum fluid, Chandler *et al.*[16,17] have applied the reference interaction site model (RISM) for molecular fluids to an isomorphic hard sphere polymer with a finite discretization P as a primitive model of the fluid helium. With a successful description of effect of spatial dispersion, their results demonstrated the applicability of RISM-type integral equation to quantum fluids. To avoid the formidable amount of numerical calculation of the $P\times P$ matrix in Chandler's work, Shinoda *et al.*[18,19] developed a scalar integral equation, which is obtained by averaging the RISM integral equation with infinite P over the whole imaginary time interval. Inspired by the ideas of Chandler and Shinoda, we model the quantum fluids in density functional theory as an isomorphic polyatomic molecule.

In recent years, DFT of polymers is well advanced. Yethiraj and Woodward[20,21] have proposed a method in which the ideal noninteracting chain system is treated via an independent Monte Carlo simulation and the weighted density approximation is used in the calculation of the excess free energy functional. Chandler *et al.*[22–24] have done similar work with the excess free energy functional derived from an integral equation theory. Based on their study, more efficient methodologies had been proposed. McCoy *et al.*[25] developed a method to take the simulation out of the iteration procedure. Recently, Yu and Wu[26] worked out a new theory that

[a]Author to whom correspondence should be addressed; Electronic mail: gaogh@mail.tsinghua.edu.cn

combines the fundamental measure theory (FMT) of Rosenfeld[27] for excluded volume effect and Wertheim's TPT1[28] for chain connectivity. Compared with the previous work, this theory has the advantage of simplicity and numerical efficiency.

In this work, a quantum hydrogen molecule is represented by a hard sphere ring model plus the van der Waals attractions. The method proposed by Yu and Wu is applied to a ringlike molecule. To make comparison, a path integral grand canonical Monte Carlo (PIGCMC) simulation is also performed to obtain the density distribution of hydrogen in single-walled carbon nanotubes. In DFT, the number of segments on the ring is a parameter of temperature, which is determined by fitting the density profiles with those of computer simulation at the same temperature and bulk density. The results of PIGCMC in this work and other available simulation data in literature are used to check the proposed model.

II. THEORY

We focus our investigation in this work on the density functional study of hydrogen adsorption at low temperatures, and in this situation, the hydrogen molecule should be treated quantum mechanically by the Feynman path integral method. An isomorphic polymer ring is introduced in density functional theory to represent the path integral configuration. The Helmholtz energy of the polymer ring consists of an ideal and an excess part. The latter part is the combination of the interactions of an inhomogeneous hard sphere, chain connectivity and the van der Waals attraction. The inhomogeneity of the fluid is caused by an external potential of cylindrical wall.

A. Path integral formalism

In PI formalism, each quantum molecule is replaced by a classical ring polymer of P beads. Each bead on a ring is coupled to adjacent beads on the same ring through harmonic springs. The polymers experience both an external potential U^{ext}, due to the other molecules in the fluid and solid, and an internal potential U^{int}, which comes from the intramolecular bonding interactions. The external interactions include simple pairwise Lennard-Jones potential between like-numbered beads on different rings and the interaction of each bead with solid surface, i.e.,

$$U^{\text{ext}}=\frac{1}{P}\sum_{\alpha=1}^{P}\sum_{i<j}^{N} V(r_{ij}^{\alpha})+\frac{1}{P}\sum_{\alpha=1}^{P}\sum_{i=1}^{N} V_{sf}(z_i^{\alpha}), \tag{1}$$

where P is the number of beads on each ring, N is the total number of molecules, $V(r_{ij}^{\alpha})$ is the pair potential between head α on molecule i and bead α on molecule j, r_{ij}^{α} denotes the scalar distance between the beads. $V_{sf}(z_i^{\alpha})$ is the interactive potential between bead α on molecule i and the solid surface, and z_i^{α} is the distance between bead α on molecule i and the solid surface. The internal potential is in the form of a harmonic interaction

$$U^{\text{int}}=\frac{Pm}{2(\beta\hbar^2)}\sum_{\alpha=1}^{P}\sum_{i=1}^{N}|r_i^{\alpha}-r_i^{\alpha+1}|^2, \tag{2}$$

where r_i^{α} is the position of bead α on ring i,m is the mass of each bead on the quantum circle. All the beads have the same mass, which is also equal to the mass of a classical hydrogen molecule, $m=3.344\times10^{-27}$ kg. $\beta=1/kT$, k is the Boltzmann constant, and $\hbar$ is the Plank constant divided by 2π. When $\alpha=P$, we have $\alpha+1=1$, as required for a ring polymer. The PI formalism is exact in the limit $P\to\infty$. In practice, the number of beads used in a simulation is increased until the properties, e.g., the total quantum energy, converge. This value of P is then used in production runs.

B. Ring polymer model in DFT

In accordance with the PI representation of quantum hydrogen, we consider in this work a ring polymer isomorphism. In PI, the quantum molecule is expressed as a ring of beads. Between adjacent beads on the same ring, there is harmonic interaction, while Lennard-Jones potential divided by P (number of beads) is applied to like numbered beads on a different ring. Accordingly, the model in this work is represented by ring polymer. And to simplify the problem, the segments on the ring are set to be tangentially connected with their neighbors, i.e., the bond length is equal to the segment diameter and there is no angular constraint between neighboring bonds. In the model, the intramolecular connection was represented by the modified Wertheim's first order perturbation theory, which will be discussed later. The number of segments varies with temperature. In practice, the bead number is decided by fitting the density profile with those from computer simulations.

Constructed from a Legendre transform of the Helmholtz energy functional, the grand potential functional Ω can be expressed as

$$\Omega[\rho(\mathbf{r})]=F[\rho(\mathbf{r})]+\int[\psi(\mathbf{r})-\mu]\rho(\mathbf{r})d\mathbf{r}, \tag{3}$$

where, $\mathbf{r}$ denotes the segment position. $\rho(\mathbf{r})$ is the segment density as a function of position. $F[\rho(\mathbf{r})]$ is the intrinsic Helmholtz energy functional. $\psi(\mathbf{r})$ represents the external potential, which is exerted by a cylindrical pore. Because of the ring configuration, all the segments on the ring are identical, and we only use $\mathbf{r}$ to represent configuration $\mathbf{R}=(\mathbf{r}_1,\mathbf{r}_2,\ldots,\mathbf{r}_M)$. Here, M is the number of segments on a ring. The equilibrium density distribution satisfies the stationary condition

$$\frac{\delta\Omega}{\delta\rho(\mathbf{r})}=0. \tag{4}$$

Helmholtz free energy functional can be expressed as a sum of an ideal gas and an excess term

$$F=F_{\text{id}}+F_{\text{ex}}. \tag{5}$$

The ideal gas term is known exactly

$$\beta F_{\text{id}}=\int d\mathbf{r}\,\rho(\mathbf{r})[\ln\rho(\mathbf{r})-1]. \tag{6}$$

Here, we neglect the bonding potential that represents the chain connectivity. This potential is essentially a discrimination of segments with different positions on a polymer chain

in inhomogeneous fluid. Whereas in the ring configuration studied in this work, all the segments on the same ring are considered identical to each other, therefore, this item is not necessarily needed.

To derive the excess Helmholtz energy functional due to intramolecular and intermolecular interactions, we follow the procedure proposed by Yu and Wu. The contribution to the excess Helmholtz energy due to the excluded volume effects is represented by the fundamental measure theory (FMT) of Rosenfeld[27] and the chain connectivity by modified version of Wertheim's TPT1.[28] Consequently, the excess Helmholtz energy functional can be expressed as

$$\beta F_{\mathrm{ex}}=\int d\mathbf{r}\{\Phi^{\mathrm{hs}}[n_\alpha(\mathbf{r})]+\Phi^{\mathrm{chain}}[n_\alpha(\mathbf{r})]\}+\beta F_{\mathrm{att}}, \quad (7)$$

where, $\Phi^{\mathrm{hs}}[n_\alpha(\mathbf{r})]$ and $\Phi^{\mathrm{chain}}[n_\alpha(\mathbf{r})]$ are, respectively, the excess Helmholtz energy densities due to hard-sphere repulsion and chain connectivity. Here, the chain connectivity term arises from the indirect interactions due to the exclude volume effects. F_{att} is the excess Helmholtz energy due to the soft attractive potential. Equation (7) implies that the effect of chain connectivity on intramolecular interactions can be accounted using only segment densities. According to FMT, the scalar and vector weighted densities are defined as

$$n_\alpha(\mathbf{r})=\int \rho(\mathbf{r}')w^{(\alpha)}(\mathbf{r}-\mathbf{r}')d\mathbf{r}', \quad (8)$$

where the subscripts $\alpha=0$, 1, 2, 3, $V1$, $V2$ denote the index of six weight functions $w^{(\alpha)}(r)$, i.e.,

$$w^{3(2)}(\mathbf{r})=\delta(d/2-r), \quad (9)$$

$$w^{(3)}(\mathbf{r})=\Theta(d/2-r), \quad (10)$$

$$\mathbf{w}^{(V2)}(\mathbf{r})=(\mathbf{r}/r)\,\delta(d/2-r), \quad (11)$$

where d represents the diameter of a hard sphere segment. $\Theta(r)$ is the Heaviside step function, and $\delta(r)$ denotes the Dirac delta function. Integration of the two scalar functions, $w^{(2)}(r)$ and $w^{(3)}(r)$, with respect to position gives, respectively, the particle surface area and volume; and integration of the vector function $\mathbf{w}^{(V2)}(\mathbf{r})$ is related to the gradient across a sphere in the $\mathbf{r}$ direction. Therefore, these three functions are directly related to the geometry of a spherical particle. The other three are proportional to them,

$$w^{(0)}(\mathbf{r})=\frac{w^{(2)}(\mathbf{r})}{\pi d^2}, \quad w^{(1)}(\mathbf{r})=\frac{w^{(2)}(\mathbf{r})}{2\pi d}, \quad \mathbf{w}^{(V1)}(\mathbf{r})=\frac{\mathbf{w}^{(V2)}(\mathbf{r})}{2\pi d}. \quad (12)$$

From Eq. (9) to (12), one can see that, all weight functions are independent of density profiles.

By using the scaled-particle differential equation, Rosenfeld derived the excess Helmholtz energy density due to hard-sphere repulsion[27]

$$\Phi^{\mathrm{hs}}\{n_\alpha(\mathbf{r})\}=\Phi_1^{\mathrm{hs}}+\Phi_2^{\mathrm{hs}}+\Phi_3^{\mathrm{hs}}, \quad (13a)$$

where

$$\Phi_1^{\mathrm{hs}}=-n_0\ln(1-n_3), \quad (13b)$$

$$\Phi_2^{\mathrm{hs}}=\frac{n_1n_2-\mathbf{n}_{V1}\cdot\mathbf{n}_{V2}}{(1-n_3)}, \quad (13c)$$

$$\Phi_3^{\mathrm{hs}}=\frac{\frac{1}{3}n_2^3-n_2\mathbf{n}_{V2}\cdot\mathbf{n}_{V2}}{8\pi(1-n_3)^2}. \quad (13d)$$

In the limit of a bulk fluid, the two vector weighted densities $\mathbf{n}_{V1}$ and $\mathbf{n}_{V2}$ vanish, and the Helmholtz energy becomes identical to that from the Percus–Yevick equation or from the scaled-particle theory.[29]

According to Wertheim's first-order perturbation theory for a bulk chain fluid, the Helmholtz energy density due to chain connectivity is given by

$$\Phi^{\mathrm{chain},b}=\frac{1-M}{M}\rho_b\ln y^{\mathrm{hs},b}(d). \quad (14a)$$

While for a ring fluid, as derived by Sear,[30] the item $(1-M)$ in the numerator could be simply replaced by $(-M)$, and the expression is modified to

$$\Phi^{\mathrm{chain},b}=-\rho_b\ln y^{\mathrm{hs},b}(d), \quad (14b)$$

where ρ_b is the segment number density and $y^{\mathrm{hs},b}(d)$ is the contact value of the cavity correlation function between segments, both in bulk status. To extend Eq. (14b) to nonuniform systems, it is assumed that the weighted densities of FMT can be similarly applied to calculate the Helmholtz energy density due to chain connectivity. Therefore, as suggested in the work of Yu and Wu,[31] ρ_b in Eq. (14b) is replaced by $n_0\zeta$ and $y^{\mathrm{hs},b}(d)$ is replaced by

$$y_{11}^{\mathrm{hs}}(d,n_\alpha)=\frac{1}{1-n_3}+\frac{n_2\,d\zeta}{4(1-n_3)^2}+\frac{n_2^2\,d^2\zeta}{72(1-n_3)^3}, \quad (15)$$

where $\zeta=1-\mathbf{n}_{V2}\cdot\mathbf{n}_{V2}/n_2^2$. Subsequently, the Helmholtz energy density due to chain formation at nonuniform conditions is

$$\Phi^{\mathrm{chain}}(n_\alpha)=-n_0\zeta\ln y^{\mathrm{hs}}(d,n_\alpha). \quad (16)$$

Equation (16) is different from that obtained from a local density approximation.

Because of the identity of segments on the same ring, the attractive potential added on the segment is equal to the total potential imposed on the molecule divided by M,

$$F_{\mathrm{att}}=\tfrac{1}{2}\int\int d\mathbf{r}\,d\mathbf{r}'\,\rho(\mathbf{r})\rho(\mathbf{r}')g(\mathbf{r},\mathbf{r}')\phi^{\mathrm{att}}(|\mathbf{r}-\mathbf{r}'|)/M. \quad (17)$$

According to the WCA potential model,

$$\phi^{\mathrm{att}}(|\mathbf{r}-\mathbf{r}'|)=\begin{cases}-\varepsilon, & |\mathbf{r}-\mathbf{r}'|\leqslant r_{\min},\\ 4\varepsilon\left(\dfrac{\sigma^{12}}{|\mathbf{r}-\mathbf{r}'|^{12}}-\dfrac{\sigma^6}{|\mathbf{r}-\mathbf{r}'|^6}\right), & r_{\mathrm{cut}}\geqslant|\mathbf{r}-\mathbf{r}'|\geqslant r_{\min},\\ 0, & |\mathbf{r}-\mathbf{r}'|<r_{\mathrm{cuin}},\end{cases} \quad (18)$$

where σ is the soft sphere diameter. $r_{\min}=\sqrt[6]{2}\sigma$ is the equilibrium distance between particles. r_{cut} is the cutoff distance. When mean field approximation is used, $g(\mathbf{r},\mathbf{r}')=1$. In WCA perturbation theory, the relation between the hard sphere and

soft sphere diameter is obtained by setting the compressibility of the hard sphere fluid equal to that of the soft sphere reference system, i.e.,

$$\int d\mathbf{r}\{y^{\mathrm{hs}}(d,r)\exp[-\beta\varepsilon_P^{\mathrm{hs}}(d,r)-1]\} = \int d\mathbf{r}\{y^{\mathrm{hs}}(d,r)\exp[-\beta\varepsilon_P^{(0)}(\sigma,r)-1]\}, \tag{19}$$

where $\varepsilon_P^{\mathrm{hs}}$ and $\varepsilon_P^{(0)}$ are, respectively, the pair interaction of hard sphere fluid and the reference system. $y^{\mathrm{hs}}(d,r) = \exp[\beta\varepsilon_P^{\mathrm{hs}}(d,r)]g^{\mathrm{hs}}(r)$ has identical forms for both hard sphere and soft sphere systems. The hard sphere diameter d, which is a function of temperature and density, can be determined from Eq. (19). However, for simplicity of programming, we ignore the temperature and density dependence of d and assume it to be σ. The same assumption has been made by Bull and Evans,[32] and Peterson *et al.*[33]

Minimization of the grand potential with respect to the density profiles yields the following Euler–Lagrange equation:

$$\rho(\mathbf{r}) = \exp[\beta\mu_M - \beta\Psi_{\mathrm{ext}}(\mathbf{r}) - \beta M\Lambda(\mathbf{r})]. \tag{20}$$

In Eq. (20), $\Lambda(\mathbf{r}) = \delta F_{\mathrm{ex}}/\delta\rho_M(\mathbf{r})$ represents an effective potential field due to intramolecular and intermolecular interactions.

When the external potential is removed, the bulk chemical potential can be derived from Eq. (20),

$$\beta\mu_M = \ln\rho_b + M\beta\mu_M^{\mathrm{hs}}(\rho_b) - M\left[\ln y_{11}^{\mathrm{hs},b}(d) + \rho_b\frac{\partial \ln y_{11}^{\mathrm{hs},b}(d)}{\partial\rho_b}\right] - \frac{32\sqrt{2}}{9}\rho_b\pi\varepsilon\sigma^3, \tag{21}$$

where, μ_M^{hs} is the excess chemical potential for corresponding hard spheres calculated from the scaled particle theory.[34]

C. Particle-wall interaction

In this work, hydrogen molecules and carbon atoms are both treated as structureless spherical particles. Both hydrogen–hydrogen and hydrogen–carbon interactions result from Lennard-Jones potential located at the mass center of the particles. The energy and size parameters of Lennard-Jones potential are 36.7 K and 0.296 nm for hydrogen, and 28.2 K and 0.335 nm for carbon, respectively. Hydrogen–carbon interactions are calculated by Lorentz–Berthelot mixing rules through parameters listed above.

For simplicity, instead of the real discrete wall, the carbon nanotube studied in this work is modeled as a structureless cylindrical pore, and the pore effect is represented by an external potential. Because there is little discrepancy between results calculated by these two methods, this kind of replacement is reasonable. As described by Stan and Cole,[35] the integration of the fluid–solid potential over the cylindrical wall results in the following expression:

$$\psi_{\mathrm{ext}}(z,R) = 3\pi\theta\varepsilon_{\mathrm{HC}}\sigma_{\mathrm{HC}}^2\left[\frac{21}{32}\left(\frac{\sigma_{\mathrm{HC}}}{R}\right)^{10}M_{11}(x) - \left(\frac{\sigma_{\mathrm{HC}}}{R}\right)^{4}M_5(x)\right], \tag{22}$$

where z is the distance between the adatom and the nearest point on the cylinder, R is the radius of the nanotube, and $x = z/R$ is the ratio of distance to radius, θ is the same surface number density, and has a value of 38 nm^{-2}, σ_{HC} is the mixed size parameter of Lennard-Jones potential between a hydrogen molecule and a carbon atom, and

$$M_n(x) = \int_0^{\pi} d\varphi\,\frac{1}{(1+x^2-2x\cos\varphi)^{n/2}}. \tag{23}$$

Simpson integration is used to get the final potential. However, it should be noted that because of the path integral and ring polymer isomorphism, the external potential acted on a single segment in GCMC and DFT is the total potential divided by M.

III. RESULTS AND DISCUSSION

Picard-type iteration is used to solve Eq. (20). The iteration starts from bulk segment density. To avoid divergence, the old and new density profiles are mixed in proportion and the iterative process continues until the percentage change is smaller than 10^{-6}. Trapezoidal integration is used with step size range from 0.01σ to 0.02σ, except for some improper integration, which is processed by the Gauss integration method.

To check the DFT proposed in this work, we perform PIGCMC to obtain the density profiles of hydrogen inside the carbon nanotubes. In PIGCMC, periodic boundary condition is applied in the axis direction. The volume of the system is adjusted through changing the length of the tube to control the number of molecules within 200 to 1000. Each molecule consists of numbers of beads connected by harmonic springs. 0.2 million configurations are used to reach the system equilibrium and another equal amount are summed up to obtain the average value.

In this work, the only parameter that could be adjusted is the number of segments, both in PIGCMC and DFT. In the former, we follow the routine work of Wang and Johnson,[3] and Gu and Gao,[12] and set the number of beads on a ring increase with the decrease of temperature. Actually, the system energy converges with the increase of bead number, and it reaches the true value with infinite bead number. In practice, the number of bead on the ring is usually increased and truncated at a certain value when there is little change of system energy. However, in DFT, the segment number M is adjusted by fitting the density profile with that obtained from PIGCMC at the same temperature and bulk density. It should be noted that, in most cases, the segment number on ring polymer (RP) in DFT is smaller than that on path integral (PI) isomorphism in PIGCMC. This is because in PI, the intramolecular distance between adjacent beads is far smaller than that in RP, which is set to be the hard sphere diameter.

According to our previous work,[12] in the PIGCMC calculation, we set 13 beads on each quantum ring at 70 K and

TABLE I. The segment number at different temperatures.

Temperature (K)	Bead number in PI	Segment number in RP	MRD (%)
70	13	4	19.62
80	12	4	16.32
90	11	3	13.45
100	10	3	12.14
110	9	3	14.57
120	8	2	21.22
130	7	2	17.61
140	6	2	18.91
150	5	2	14.65
160	4	2	20.19
170	3	2	27.28
180	2	1	8.12
190	1	1	1.89
200	1	1	1.07

the number decreases proportionally with the increase of temperature, until it becomes unit at 190 K. Within the same temperature range, the number of segments on the ring polymer in DFT decreases from 4 to 1.

It is known from a previous investigation of a path integral simulation in Gibbs ensemble that the phase diagram simulated via PI method agrees well with experimental results, while classical simulation gives large errors. This proves that the PI method is valid for hydrogen. On the other hand, through the calculation, the bead number to each temperature in PI is determined.

The numbers of beads in PI and segments in RP are listed in Table I. The numbers of segments on the ring polymer in DFT are decided by fitting density profiles with that of PIGCMC. The fitting procedure is carried out in a (30, 30) tube with a reduced bulk density of 0.2. It is shown from Table I that the segment number decrease with the decrease of PI bead number, and both have an inverse relation to temperature. When the temperature is high, for example, 190 K, both numbers reduce to unit, which is the classical case. The inside-tube volume is divided into 250 layers along radius direction. The maximum relative deviations (MRD) between DFT and PIGCMC of all the layers are also listed in Table I. Most of the large errors are located at the crest and trough in the density profile, especially for the later. This is because we set the segment number, which is in close relation to the height of the maximum and minimum points as integers. Moreover, the fluctuation in PIGCMC also contributes to the deviation.

In Fig. 1, the density profiles calculated from our DFT are compared to that from Johnson's GCMC.[3] Four segments are set on the ring polymer in our calculation. It should be pointed out that, in Johnson's work, the intermolecular potential and the corresponding parameters are slightly different from that described in this paper. To make a comparison with their work, the results in this figure are calculated by the size parameters ($\sigma_H = 0.3075$ nm and $\sigma_C = 0.343$ nm) listed in their paper. Another difference between the two pieces of work is that we do not consider the interstitial adsorption while Johnson did, since a two-dimensional DFT calculation is very time consuming. But as claimed in Ref. 2, the outside

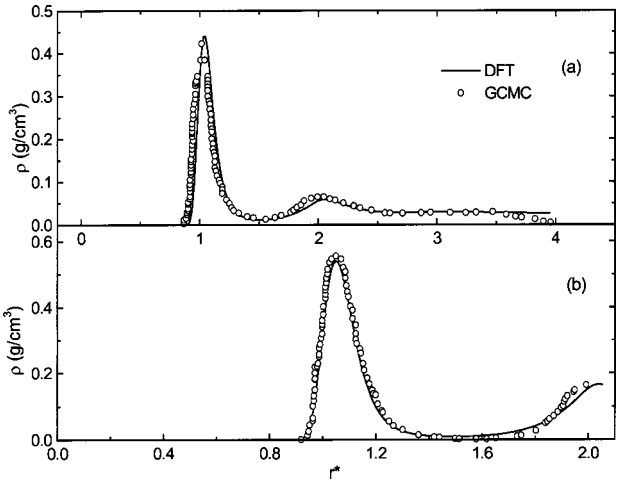

FIG. 1. Comparison between DFT in this work and computer simulation in Ref. 2 for the density profiles at 77 K and 50 atm: (a) (18, 18) tube density and (b) (9,9) tube density.

particles have little effect on those inside the tube. In particular for the (9, 9) tube, there is no interstitial adsorption at all. As a result, our DFT data agree well with their simulation.

The computer simulation or experiment on hydrogen adsorption at low temperature is rarely available in the literature. To check the validity of our theory, we also carried out PIGCMC simulation in this work. The details of our PIGCMC simulation has been described elsewhere.[12] Figures 2–4 show comparisons between the density profiles obtained

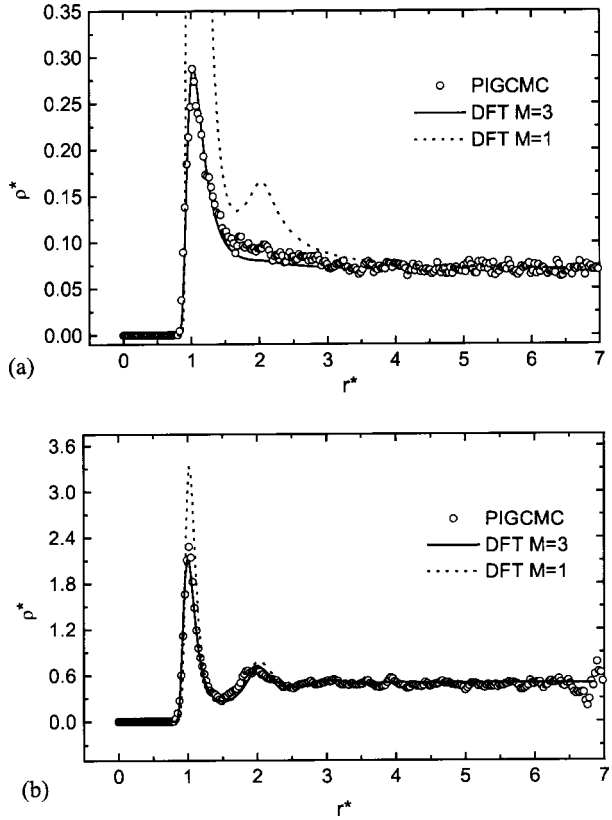

FIG. 2. Density profiles inside (30,30) tube: the temperature is 100 K; the reduced bulk density is (a) 0.08 and (b) 0.5.

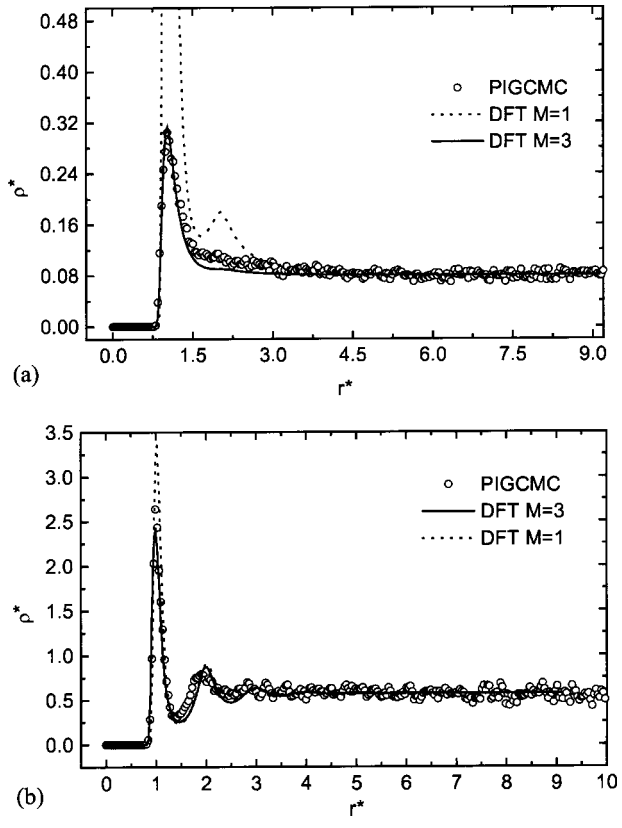

FIG. 3. Density profiles inside (40,40) tube: the temperature is 100 K; the reduced bulk density is (a) 0.08 and (b) 0.5.

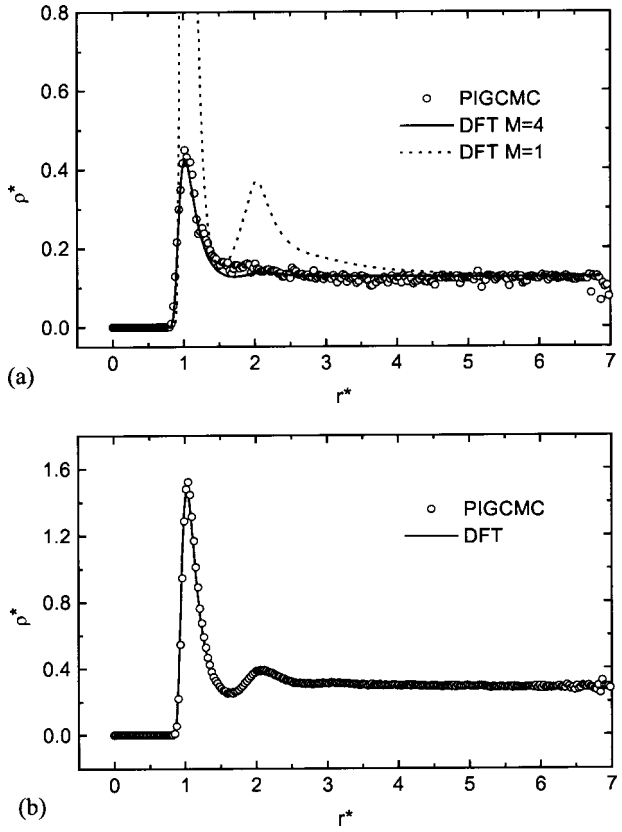

FIG. 4. Density profiles inside (30,30) tube: (a) $\rho^*=0.12$, $T=70$ K; (b) $\rho^*=0.3$, $T=200$ K.

from density functional theory and those from computer simulation. The dotted lines are the classical results with only one segment number. It is clear from these figures that, the ring polymer model makes good representation of the path integral isomorphism by giving a reasonable agreement with simulation results in a wide range of temperature and density, while the classical DFT (the case when segment number is equal to unit) diverges a lot at low temperatures. However, at high temperature [see Fig. 4(b)], the segment number becomes unit, and only one line is plotted to represent the DFT result. Moreover, with the increase of density, the discrepancy between the ring polymer (quantum) and the classical DFT diminished. The same rule also applies to quantum rings in path integral isomorphism. This can be explained by the behavior of a ring polymer. There are two factors that affect the density distribution, one is the chain connectivity, and the other is the packing effect. At low density, the former factor dominates. While at high density, the packing effects resulted from the total number of hard spheres dominates, and the relation between the segment number and the density profile becomes indifferent.

In Figs. 5 and 6, the adsorption isotherms inside the carbon nanotubes are calculated via density functional theory. Three sizes of armchair tubes, (30, 30), (35, 35), and (40, 40) are studied. Here, both the total and the excess adsorption are presented. The total adsorption is calculated by

$$\Gamma=\frac{2\int_0^R\rho(r)r\,dr}{R^2}, \tag{24}$$

and the excess adsorption is

$$\Gamma_{\mathrm{ex}}=\frac{2\int_0^R(\rho(r)-\rho_{\mathrm{bulk}})r\,dr}{R^2}, \tag{25}$$

where, ρ_{bulk} is the bulk density and R is the radius of the tube. It should be noticed that this definition does not correspond to the excess adsorption generally used in the experiment. It is introduced to explain the effect on the amount of adsorption caused by only the particle-wall interactive potential other than space.

In Fig. 5, the total amount of adsorption increases with pressure and decreases with temperature. At the same temperature, conceptually, the larger tube should hold more particles. However, as shown in the figure, this trend is not so evident. The reason could be explained from Fig. 7, in which the particle-tube interactive potential is plotted. Besides space, this interaction is another important factor to affect the amount of adsorption. In Fig. 7, the location that has the minimum potential is the equilibrium position, and accordingly, the potential value at this position affects the amount of adsorption dramatically. From the figure, one can see that the absolute value of potential has an inverse relation to tube radius. Therefore, the increase of tube size has a negative contribution to this part of interaction.

The effect of particle-tube interaction is more evident for the excess adsorption, which is shown in Fig. 6. In the figure, the excess adsorption decreases monotonically with tube size due to the inverse relation between tube radius and the particle-wall interaction. While to each tube, Γ_{ex} has a maxi-

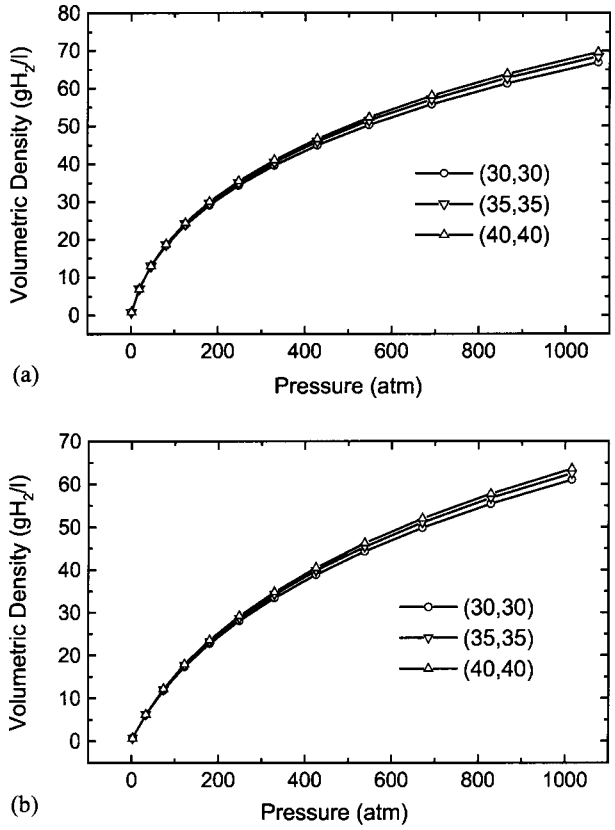

FIG. 5. The total amount of adsorption isotherms obtained DFT: (a) at 100 K; (b) at 150 K.

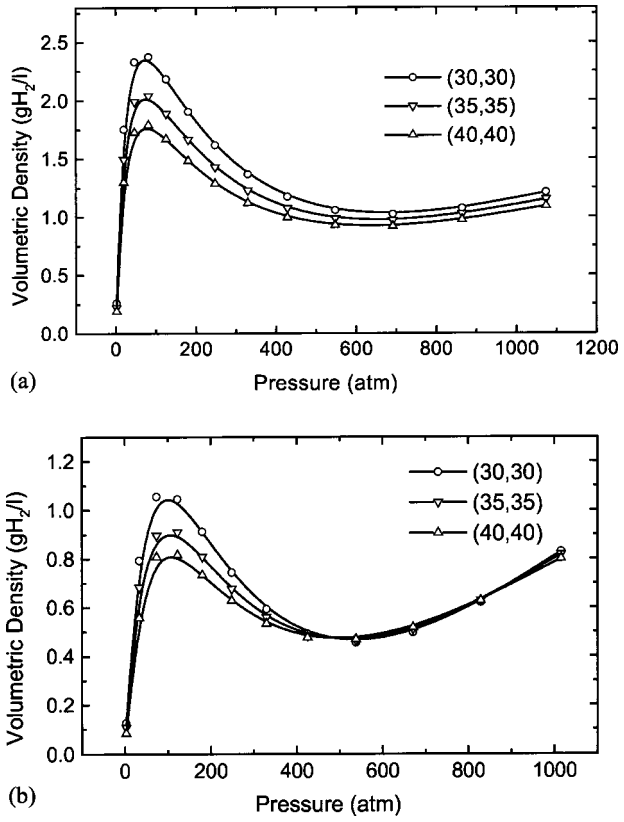

FIG. 6. The excess adsorption isotherms obtained from DFT: (a) at 100 K; (b) at 150 K.

mum at 100 K and 81 atm, and 150 K and 122 atm. The two pressures correspond to reduced bulk density about 0.15. Then, with the increase of pressure, the adsorption decreases toward a minimum and then reincreases slightly. The qualitative behavior is similar to that previously found for nitrogen[6] and krypton.[36] As explained by Darkrim,[6] there are two competing effects that control the outcome of Γ_{ex}: the repulsive interaction between gas molecules at short distances and the strong attractive interaction between these molecules and the substrate. At low pressure, the attractive interaction dominates, so the higher the pressure, the larger the amount of excess adsorption. While at high pressure, the increase of adsorption with pressure is limited by the effect of repulsive intermolecular interactions, which makes the behavior more like that of hard spheres. It can also be seen from the isotherms that the optimized amount of excess adsorption is 2.37 gH_2/L. However, because only adsorption inside the tube is considered in this work and the interstitial uptake is not included, the effect of which is still not clear. While with an inter-tube separation of 0.315 nm,[37] which is far smaller than the tube diameter [a (30, 30) tube has a diameter of 4.06 nm], the interstitial region is supposed to give relatively low usable capacity ratios.

IV. CONCLUSIONS

In this work, a density functional theory that is based on the combination of fundamental-measure theory of Rosenfeld for inhomogeneous hard spheres and modified version of Wertheim's thermodynamic perturbation theory for bulk hard-sphere ring as well as WCA approximation of van der Waals attractions is used to represent the quantum hydrogen molecule at low temperatures. The density functional is tested by PIGCMC simulation results of both this work and those available in the literature. Good agreement is achieved for the density profile inside the tube.

Using the proposed DFT, we also calculated the total and excess adsorption isotherms of hydrogen in (30, 30), (35, 35), and (40, 40) armchair nanotubes at 100 and 150 K. Results show that the volumetric density of total adsorption increases monotonically with the increase of pressure and the decrease of temperature. The excess adsorption has a maximum value at 100 K and 81 atm, and 150 K and 122 atm. Moreover, within the range of tube size studied in this work,

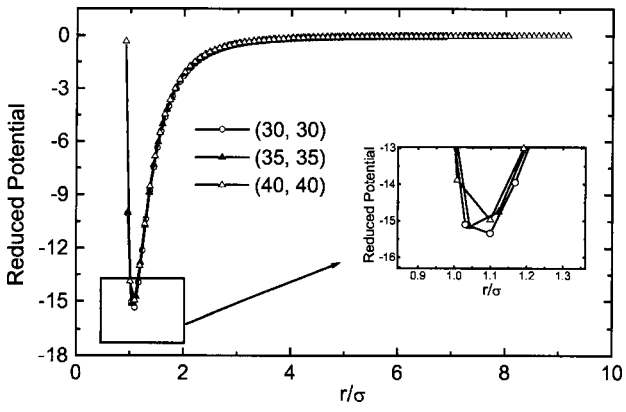

FIG. 7. The particle-wall potentials of (30, 30), (35, 35) and (40, 40) tubes.

the excess adsorption has an inverse relation to tube radius. This is due to the decrease of particle-wall interaction in larger tubes.

Although this theory provides a good substitution of quantum molecule in most of the cases, there are still some situations, in which the change of segment number cannot give a good adjustment to the appearance of the density profile, because we do not adopt a fraction segment number. A modified version of intrinsic Helmholtz energy for hard-sphere repulsive part[38] and a fused hard sphere ring model may make some improvement to the current problem. An inclusion of harmonic interaction may also give a better result. Further investigation on this topic is being carried out.

ACKNOWLEDGMENTS

The work is supported by grants from the Tsinghua University Fundamental Research Foundation (Grant No. JC200015004) and the Beijing Key Laboratory of Green Chemical Reaction Engineering and Technology. We would also like to thank Dr. Jianzhong Wu for providing Y.-X. Yu financial support to accomplish some subroutines used in this work.

[1] A. C. Dillon, K. M. Jones, T. A. Bekkedahl, C. H. Kiang, D. S. Bethune, and M. J. Heben, Nature (London) **386**, 377 (1997).
[2] Y. Ye, C. C. Ahn, C. Witham, B. Fultz, J. Liu, A. G. Rinzler, D. Colbert, K. A. Smith, and R. E. Smalley, Appl. Phys. Lett. **74**, 2307 (1999).
[3] Q. Y. Wang and J. K. Johnson, J. Chem. Phys. **110**, 577 (1999).
[4] Q. Y. Wang and J. K. Johnson, J. Phys. Chem. B **103**, 4809 (1999).
[5] F. Darkrim and D. Levesque, J. Chem. Phys. **109**, 4981 (1998).
[6] F. Darkrim, J. Vermesse, P. Malbrunot, and D. Levesque, J. Chem. Phys. **110**, 4020 (1999).
[7] M. Rzepka, P. Lamp, and M. A. de la Casa-Lillo, J. Phys. Chem. B **102**, 10894 (1998).
[8] K. Tada, S. Furuya, and K. Watanabe, Phys. Rev. B **63**, 155405 (2001).
[9] P. A. Gordon and P. B. Saeger, Ind. Eng. Chem. Res. **38**, 4647 (1999).
[10] F. Darkrim, P. Malbrunot, and G. P. Tartaglia, Int. J. Hydrogen Energy **27**, 193 (2002).
[11] R. P. Feynman and A. R. Hibbs, *Quantum Mechanics and Path Integral* (McGraw-Hill, New York, 1965).
[12] C. Gu and G. H. Gao, Phys. Chem. Chem. Phys. **4**, 4700 (2002).
[13] J. D. Mccoy, S. W. Rick, and A. D. J. Haymet, J. Chem. Phys. **90**, 4622 (1989).
[14] J. D. Mccoy, S. W. Rick, and A. D. J. Haymet, J. Chem. Phys. **92**, 3034 (1990).
[15] S. W. Rick, J. D. Mccoy, and A. D. J. Haymet, J. Chem. Phys. **92**, 3040 (1990).
[16] D. Chandler and P. G. Wolynes, J. Chem. Phys. **74**, 4078 (1981).
[17] K. S. Schweizer, R. M. Stratt, D. Chandler, and P. G. Wolynes, J. Chem. Phys. **75**, 1347 (1981).
[18] K. Shinoda, S. Miura, and S. Okazaki, J. Chem. Phys. **114**, 7497 (2001).
[19] K. Shinoda, S. Miura, and S. Okazaki, J. Chem. Phys. **115**, 4161 (2001).
[20] A. Yethiraj and C. E. Woodward, J. Chem. Phys. **102**, 5499 (1995).
[21] A. Yethiraj, J. Chem. Phys. **109**, 3269 (1998).
[22] D. Chandler, J. D. Mccoy, and S. J. Singer, J. Chem. Phys. **85**, 5971 (1986).
[23] D. Chandler, J. D. Mccoy, and S. J. Singer, J. Chem. Phys. **85**, 5977 (1986).
[24] J. D. Mccoy, S. J. Singer, and D. Chandler, J. Chem. Phys. **87**, 4853 (1987).
[25] J. B. Hooper, J. D. McCoy, and J. G. Curro, J. Chem. Phys. **112**, 3090 (2000).
[26] Y. X. Yu and J. Wu, J. Chem. Phys. **117**, 2368 (2002).
[27] Y. Rosenfeld, Phys. Rev. Lett. **63**, 980 (1989).
[28] M. S. Wertheim, J. Chem. Phys. **87**, 7323 (1987).
[29] J. P. Hansen and I. R. McDonald, *Theory of Simple Liquids*, 2nd ed. (Academic, London, 1990).
[30] R. P. Sear and G. Jackson, Mol. Phys. **81**, 801 (1994).
[31] Y. X. Yu and J. Wu, J. Chem. Phys. **116**, 7094 (2002).
[32] P. C. Ball and R. Evans, Mol. Phys. **63**, 159 (1988).
[33] B. K. Peterson, K. E. Gubbins, G. S. Heffelfinger, U. Marini, B. Marconi, and F. Vanswol, J. Chem. Phys. **88**, 6487 (1988).
[34] Y. Rosenfeld, J. Chem. Phys. **89**, 4272 (1988).
[35] G. Stan and M. W. Cole, Surf. Sci. **395**, 280 (1998).
[36] J. Vermesse and D. Levesque, J. Chem. Phys. **101**, 9063 (1994).
[37] R. Saito, G. Dresselhaus, and M. S. Dresselhaus, *Physical Properties of Carbon Nanotubes* (Imperial College Press, London, 1998).
[38] Y. X. Yu and J. Wu, J. Chem. Phys. **117**, 10156 (2002).